Structure
Article

Structural Insight into the Recognition of the H3K4me3 Mark by the TFIID Subunit TAF3

Hugo van Ingen,[1] Frederik M.A. van Schaik,[2] Hans Wienk,[1] Joost Ballering,[1] Holger Rehmann,[2] Annemarie C. Dechesne,[3] John A.W. Kruijzer,[3] Rob M.J. Liskamp,[3] H.Th. Marc Timmers,[2] and Rolf Boelens[1,*]
[1]Bijvoet Centre for Biomolecular Research, Utrecht University, 3584 CH Utrecht, The Netherlands
[2]Department of Physiological Chemistry, University Medical Centre Utrecht, 3584 CG Utrecht, The Netherlands
[3]Department of Medicinal Chemistry and Chemical Biology, Utrecht University, 3584 CH Utrecht, The Netherlands
*Correspondence: r.boelens@uu.nl
DOI 10.1016/j.str.2008.04.015

SUMMARY

Trimethylation of lysine residue K4 of histone H3 (H3K4me3) strongly correlates with active promoters for RNA polymerase II-transcribed genes. Several reader proteins, including the basal transcription factor TFIID, for this nucleosomal mark have been identified. Its TAF3 subunit specifically binds the H3K4me3 mark via its conserved plant homeodomain (PHD) finger. Here, we report the solution structure of the TAF3-PHD finger and its complex with an H3K4me3 peptide. Using a combination of NMR, mutagenesis, and affinity measurements, we reveal the structural basis of binding affinity, methylation-state specificity, and crosstalk with asymmetric dimethylation of R2. A unique local structure rearrangement in the K4me3-binding pocket of TAF3 due to a conserved sequence insertion underscores the requirement for cation-π interactions by two aromatic residues. Interference by asymmetric dimethylation of arginine 2 suggests that a H3R2/K4 "methyl-methyl" switch in the histone code dynamically regulates TFIID-promoter association.

INTRODUCTION

Modification of the nucleosomal histone proteins influences fundamental processes such as DNA transcription, repair, and replication (Kouzarides, 2007). Also, histone modifications are assumed to play an important role in the epigenetic memory of the cell. These modifications are located in the exposed N-terminal tails of the histone proteins, where several amino acids can be enzymatically modified in a number of ways. One of these modifications involves the mono-, di-, or trimethylation of the side chain amine moiety of specific histone lysine residues (Sims and Reinberg, 2006; Ruthenburg et al., 2007). Such nucleosomal marks can create interaction sites for specific reader proteins that promote or inhibit DNA-mediated processes (Kouzarides, 2007). The biochemical information embedded within these posttranslational modifications has been called the histone code (Strahl and Allis, 2000; Fischle et al., 2003).

Methylation of lysine residue K4 of histone H3 (H3K4) is correlated with the transcriptional activation of genes and is a strong predictor for RNA polymerase II promoters (Santos-Rosa et al., 2002). In particular, the trimethylated form of H3K4 (H3K4me3) is found primarily around the transcription start sites of active genes (Barski et al., 2007; Guenther et al., 2007). More insight into its relationship with transcriptional activity has come from the identification of several proteins that recognize H3K4me3. These proteins are implicated in chromatin-modifying activities and are connected to transcriptional activation. For instance, the BPTF and CHD1 proteins are subunits of chromatin-remodeling complexes and are associated with the initiation or elongation phase of transcription, respectively (Flanagan et al., 2005; Sims et al., 2005; Wysocka et al., 2006). Other reader proteins are part of complexes that add or remove other posttranslational histone modifications. For example, the repressive trimethylated H3K9 mark is removed from H3K4me3-marked nucleosomes by JMJD2A (Huang et al., 2006). Interestingly, the human ING2 tumor suppressor is a subunit of the mSin3/HDAC corepressor complex, suggesting a signaling pathway for silencing activated genes (Shi et al., 2006). A related ortholog from yeast, Yng1, is part of the NuA3 histone acetyl transferase (HAT) complex and provides a connection to transcriptional activation (Taverna et al., 2006). Recently, H3K4me3 was also linked to DNA recombination via direct association with the V(D)J recombinase component RAG2 (Matthews et al., 2007; Ramon-Maiques et al., 2007). These "reader" proteins bind to methylated H3K4 by using either chromodomains and tudordomains of the Royal family (in the case of CHD1 and JMJD2A), or by using plant homeodomain (PHD) fingers (in the case of BPTF, ING2/Yng1, and RAG2). Structures of these domains in complex with H3 peptides carrying H3K4me3 were reported recently (Flanagan et al., 2005; Sims et al., 2005; Huang et al., 2006; Li et al., 2006; Pena et al., 2006; Taverna et al., 2006; Matthews et al., 2007; Ramon-Maiques et al., 2007), providing a basic understanding of the structural basis of H3K4me3 recognition (Ruthenburg et al., 2007).

Recently, a direct link between H3K4me3 and the basal RNA polymerase II transcription machinery was discovered (Vermeulen et al., 2007). TAF3 (TATA box-binding protein-associated factor) is an integral subunit of the basal transcription factor TFIID. Metazoan, but not protozoan, TAF3 contains a C-terminally located PHD finger, which binds with high affinity and specificity to H3K4me3. This interaction may serve to anchor TFIID to activated promoters. Alternatively, H3K4me3 recruits TFIID via TAF3 during promoter activation, which may be particularly important for promoters lacking a canonical TATA box. Here, we investigate the molecular basis of the TAF3-H3K4me3 interaction

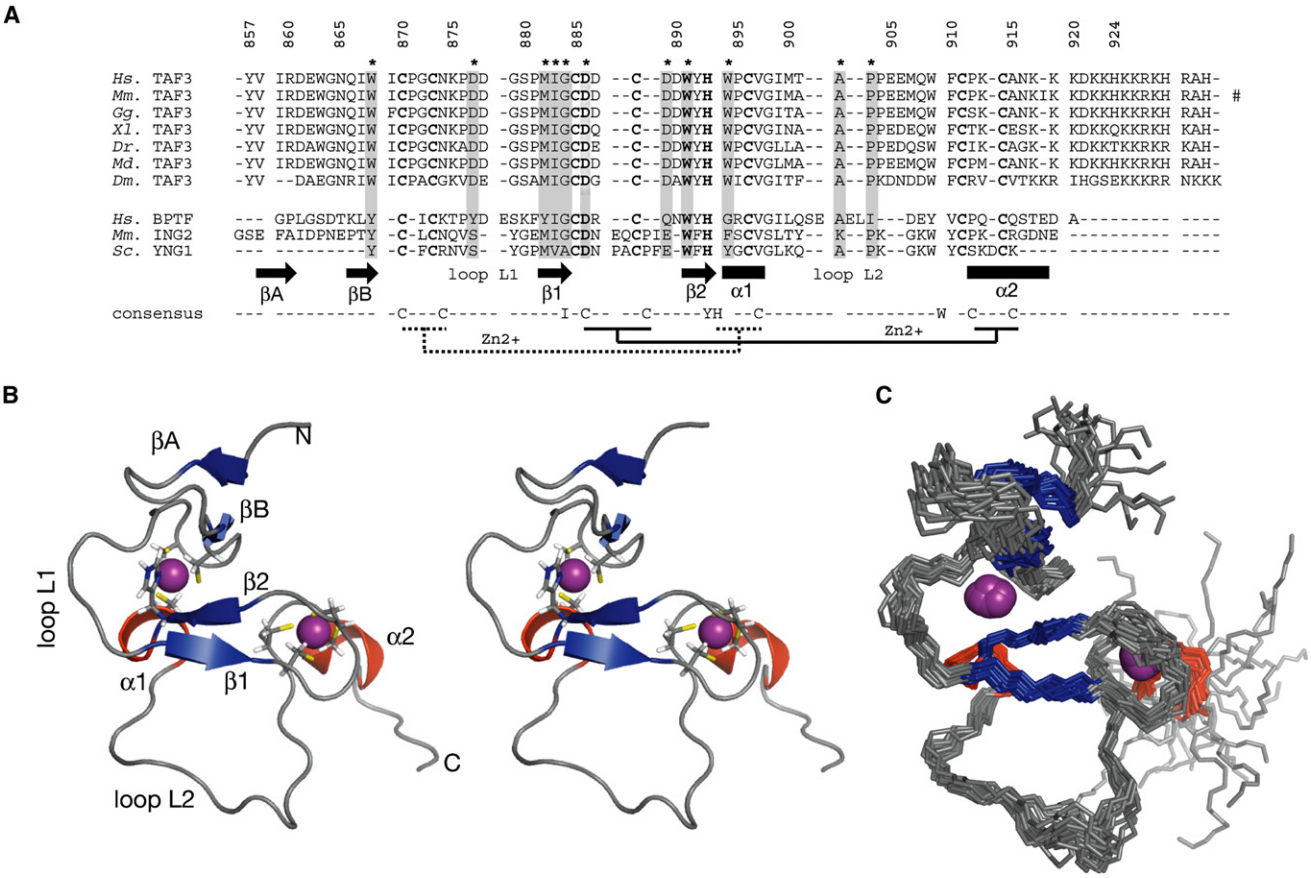

Figure 1. Sequence and Solution Structure of the TAF3-PHD Finger and Interaction with H3K4me3

(A) Structure-based sequence alignment of TAF3-PHD finger sequences and the PHD domains of BPTF, ING2, and Yng1 (*Hs*., *Homo sapiens*; *Mm*., *Mus musculus*; *Gg*., *Gallus gallus*; *Xl*., *Xenopus laevis*; *Dr*., *Danio rerio*; *Md*., *Monodelphis domestica*; *Dm*., *Drosophila melongaster*; *Sc*., *Saccharomyces cerevisiae*). In bold, conserved residues; asterisks, residues important for interaction with H3K4me3. Secondary structure elements of the TAF3-PHD finger, together with the PHD consensus sequence and the zinc-binding mode, are shown. Numbering refers to the *Mm*. TAF3, indicated with a hash.

(B and C) (B) Stereoview of the lowest-energy structure and (C) backbone traces of the ensemble of 20 structures of the free TAF3-PHD finger (residues 857–924). Color coding: β strands, blue; α helices, red; zinc, purple. Side chains of the zinc-binding residues are shown with sticks. Secondary structure elements are labeled. All structure images were made by using PyMOL (DeLano Scientific LLC, 2008).

by using NMR spectroscopy, mutational analysis, and affinity measurements. We show that due to a conserved amino acid insertion in the K4me3-binding pocket, its local structure is adjusted to fulfill the requirement for two aromatic residues to coordinate the trimethylated amino group. Furthermore, our results demonstrate that cation-π interactions involving these residues outweigh the conserved negative charge in the K4me3-binding pocket in determining methylation-state specificity. Finally, our data indicate that interference with the TAF3-H3K4me3 interaction by asymmetric dimethylation of H3R2 is caused by steric clashes and disruption of intermolecular hydrogen bonds.

RESULTS

Solution Structure of the TAF3-PHD Finger and Its Interaction with H3K4me3

The primary sequence of the TAF3-PHD finger is well conserved among metazoan species, although it is only ~30% identical to the BPTF, ING2, or Yng1 and ~15% identical to the RAG2-PHD finger (Figure 1A). The backbone traces of the lowest-energy structure and the ensemble of structures of the free TAF3-PHD finger domain are shown in Figures 1B and 1C. Structural statistics are reported in Table 1 and Table S1, available online. Overall, free TAF3-PHD is folded as a canonical PHD finger (Pascual et al., 2000; Bienz, 2006). The core of the domain is formed by a short, two-stranded antiparallel β sheet, connecting the two interleaved zinc-binding sites and α helices α1 and α2. The PHD fold contains two relatively long loops: loop L1 precedes the central β sheet, and loop L2 connects the two α helices. Heteronuclear $\{^1H\}$-^{15}N NOE values indicate that the core is characterized by a rigid backbone, whereas residues 905–908 of loop L2 and the turn between β strands β1 and β2 are more flexible, correlating with the lower structural definition of these regions in the ensemble of structures (see Figure S1). A distinctive feature of the TAF3-PHD finger compared to other PHD fingers is the presence of a second antiparallel β sheet in the N-terminal part of the domain formed by strands βA (residues

Table 1. Structural Statistics for the Free TAF3-PHD Finger and theTAF3-PHD:H3K4me3 Complex

	Free PHD Domain	H3K4me3 Complex
Restraint Information		
Total number of experimental distance restraints	1208	1644
PHD domain (intraresidual/sequential/medium/long)	355/373/172/308	318/373/199/398
H3 peptide (intraresidual/sequential/medium/long)	-	160/47/7/0
Intermolecular restraints	-	142
Zinc coordination restraints	20	20
TALOS-derived dihedral angle restraints ϕ/ψ	23/26	30/34
CSI-derived dihedral angle restraints ϕ/ψ	-	3/3
Average Rms Deviation from Experimental Restraints		
All experimental distance restraints (Å)	0.013 ± 0.002	0.013 ± 0.002
All dihedral angle restraints (°)	0.19 ± 0.12	0.18 ± 0.16
Coordinate Rms Deviation (Average to Mean, Å)		
Ordered backbone atoms	0.59	0.49
Ordered heavy atoms	0.92	0.82
Global backbone atoms	2.07	1.64
Global all heavy atoms	2.77	2.25
Ramachandran Quality Parameters (%)		
Residues in most favored regions	82.6 ± 4.7	83.0 ± 4.5
Residues in allowed regions	14.8 ± 4.9	13.5 ± 4.0
Residues in additionally allowed regions	1.5 ± 1.5	2.3 ± 2.1
Residues in disallowed regions	1.1 ± 1.5	1.1 ± 1.1

Statistics are given for residues 857–924 of TAF3-PHD and residues 1–7 of the H3K4me3 peptide. Ordered regions are residues 867–903 and 909–918 of the PHD domain.

858–860) and βB (residues 866–868). This additional sheet is rather flexible according to its reduced NOE values (average 0.58 ± 0.03).

It was shown previously that the PHD finger of TAF3 binds with high affinity to a biotinylated 17-mer H3K4me3-derived peptide (K_D = 0.16 μM) (Vermeulen et al., 2007). Here, we used a nonbiotinylated H3-derived peptide comprising residues 1–13 and determined a dissociation constant (K_D) of 0.31 ± 0.09 μM by using tryptophan fluorescence binding experiments (Figure 2A). NMR titration experiments provided support for a tight binding reaction, as many resonances of the PHD finger were in the slow-to-intermediate exchange regime (Figure S2). Binding of H3K4me3 changes the overall appearance of the spectrum, indicating that a large surface area of the PHD domain, comprising the central β sheet, the L2 loop, and the β1β2 turn, is involved in the interaction with the histone tail fragment (Figures 2B and 2C).

Solution Structure of theTAF3-PHD:H3K4me3 Complex

Using isotope-filtered NMR experiments, we obtained 140 intermolecular distance restraints between the H3K4me3 peptide and the PHD domain (Figure 2D), enabling us to solve the solution structure of the complex (Figures 3A and 3B; cf. Table 1 for the structural statistics). Residues 1–6 of the histone peptide dock tightly to the interaction surface of the PHD domain, resulting in ±1170 $Å^2$ total buried surface area upon complex formation (Figure 3C; Figure S3). The histone tail adopts a β strand conformation, forming a three-stranded antiparallel β sheet with the PHD finger by intermolecular hydrogen bonds between residues K4 and M882 and R2 and G884 (see Table S2 for a detailed analysis). The trimethyl-lysine side chain is bound in a 4-residue pocket containing two aromatic residues, coinciding with the region with the largest chemical-shift perturbation. Two sides of this pocket are formed by the side chains of W868 and "dividing" tryptophan W891, separating the K4- and R2-binding pockets. The floor is formed by residue M882, whose electron-rich thioether group contacts the trimethylated amine of K4me3. The remaining side is formed by the small D877, resulting in a rather open pocket (Figure 3D). The proximity of its negatively charged carboxylate group and the trimethylated amino group creates a favorable electrostatic interaction. Furthermore, there are contacts to R2 and the N terminus. The R2 side chain is oriented toward a negatively charged pocket formed by residues D889 and D886, consistent with the observed chemical-shift perturbation for these residues (Figure 2C) and the reduction of backbone flexibility in this region (Figure S1). Intermolecular hydrogen bonds between R2 and D889 are present in 30% of the structures in the ensemble (Table S2). The orientation of the R2 side chain, however, is poorly defined in the ensemble (Figure S3), as we did not observe signals from protons in the guanidinium group. The N terminus is hydrogen bonded to the main chain at residue 907 and to the side chain of D886. In addition, the hydrophobic methyl side chains of T3 and A1 are deeply buried in the groove formed by I883 (β1 strand), W894 (α1 helix), A902, P903, and W909 (all-L2 loop), resulting in a reduction of flexibility of the L2 loop (Figure S1). Interactions between residues Q5 and P881 and the hydrogen bond between the side chain hydroxyl group T6 and the side chain of D877 define the C-terminal end

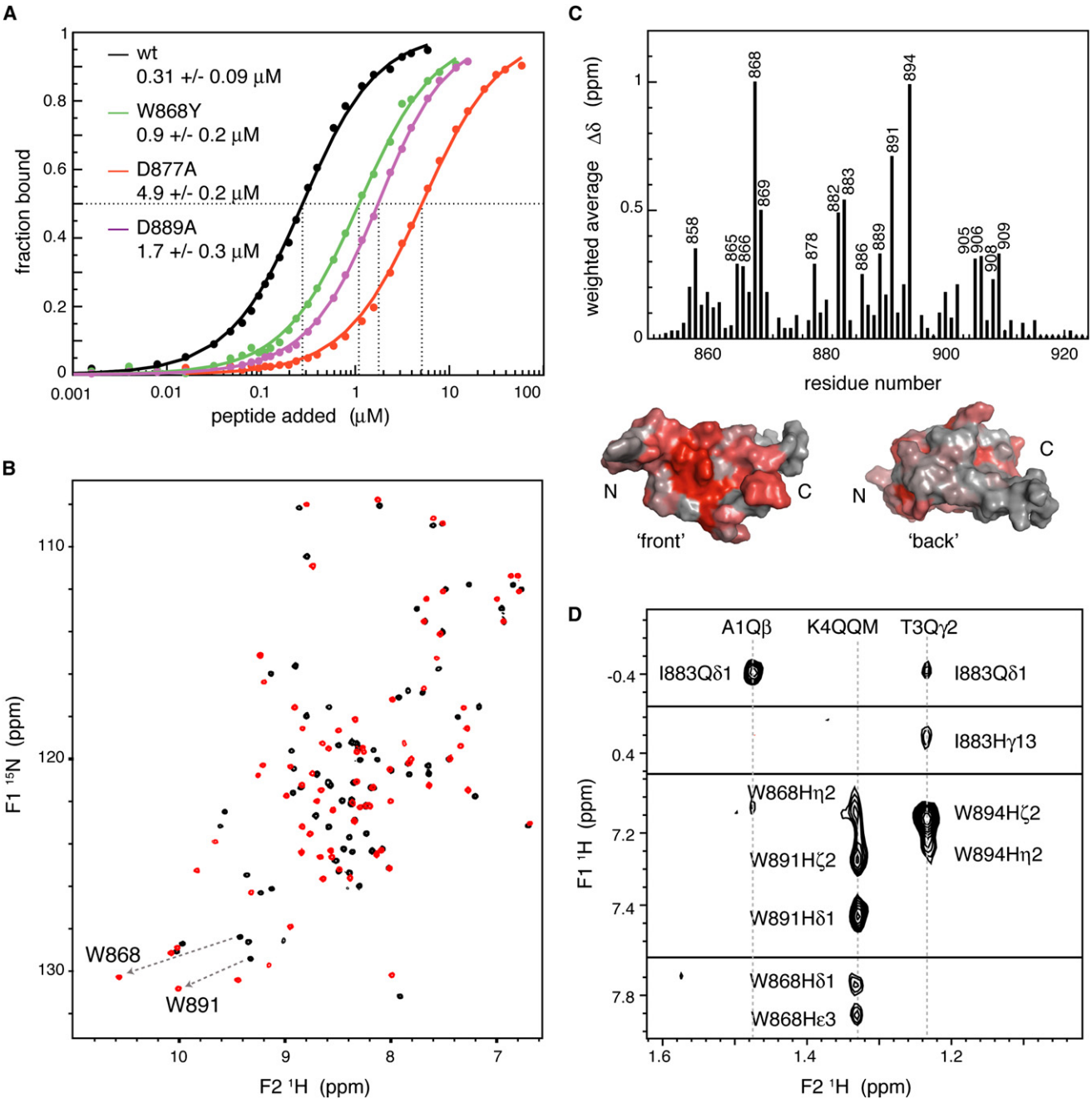

Figure 2. Interaction between the TAF3-PHD Finger and H3K4me3

(A) Tryptophan fluorescence-based binding curves and the determined dissociation constants and standard deviations for the interaction of H3K4me3 and wild-type TAF3-PHD finger or the mutants W868Y, D877A, and D889A.

(B) ^{1}H-^{15}N HSQC spectra of the free (black) and H3K4me3-bound (red) TAF3-PHD finger, indicating shifts of the indole resonances of W868 and W891.

(C) Chemical-shift perturbation (Δδ) between the free and H3K4me3-bound PHD finger, based on ^{1}H-^{15}N HSQC spectra. Surface plots of the free PHD finger are colored from gray (Δδ = 0) to red (Δδ = 0.5). Residues with significant shifts (Δδ > 10% trimmed mean + 1σ) are labeled.

(D) Sections from the ^{1}H-^{1}H plane of the ^{13}C-edited-filtered HSQC-NOESY of the TAF3-H3K4me3 complex showing intermolecular NOEs to the methyl group of A1, T3, and the degenerate methyls of K4me3 (indicated as QQM).

of the interface. Residues 8–13 of the peptide are unstructured and highly flexible, judging from the lack of sequential and medium-range NOE crosspeaks and the intense appearance of TOCSY crosspeaks for this region (data not shown). Overall, this interaction mode agrees with the characteristics of H3K4me3 recognition that were defined previously (Ruthenburg et al., 2007).

Superposition of the free and bound structure of the TAF3-PHD finger results in a backbone rms deviation of 0.9 Å (ordered regions, residues 867–903 and 909–918), indicating that binding

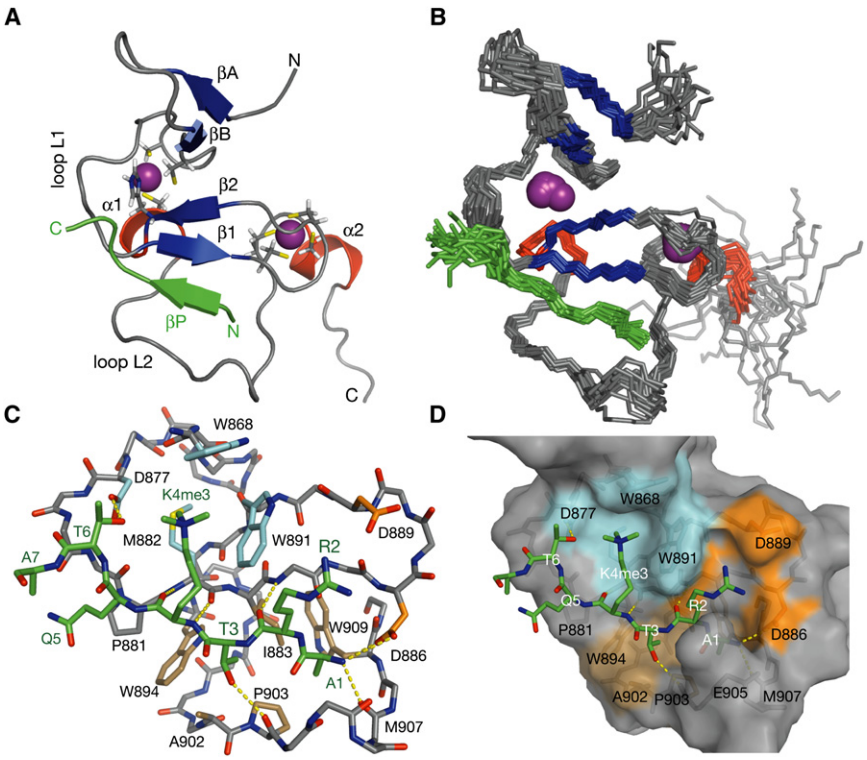

Figure 3. Solution Structure of the TAF3-PHD:H3K4me3 Complex

(A and B) (A) Lowest-energy structure and (B) backbone traces of the ensemble of 20 structures. Color coding is as for the free PHD finger; the H4K4me3 peptide (residues 1–7) is colored green. (C and D) Zoom on the interface in the TAF3-PHD:H3K4me3 structure. The PHD finger and the H3K4me3 peptide are shown in stick representation in (C); a surface plot of the PHD finger is shown in (D).

Intermolecular hydrogen bonds are indicated as yellow, dashed lines. Color coding: gray, PHD finger; cyan, K4 pocket; orange, R2 pocket; light brown, T3 and A1 pocket.

induces little change in the global conformation (Figure S4). The orientation of most side chains in the interface is preserved upon complex formation, with the exception of rotations of residues D886 and W868, correlating with their involvement in intermolecular interactions.

Mutational Analysis of the Interface

The previously described loss-of-binding mutations M882A, W891A/D890A, and D886A (Vermeulen et al., 2007) can be well explained by our structure of the TAF3-PHD:H3K4me3 complex. Alanine substitutions of M882 and W891 severely disrupt the K4me3 pocket, whereas mutant D886A cannot make an electrostatic interaction with R2 and is incapable of hydrogen bonding the N terminus of the histone tail (cf. Figure 3C). To further verify the interaction interface, we designed mutants D877A, D889A, and W868Y and measured their binding affinity by tryptophan fluorescence. In agreement with our structure, all three mutants show significant loss in binding affinity (see Figure 2A). Mutant D877A, targeting the electrostatic interaction in the K4me3 pocket and the hydrogen bond with T6, was 16-fold less effective in binding H3K4me3. The binding affinity of mutant D889A was five-fold lower than for the wild-type PHD finger (Table 2), supporting its interaction with R2. The conservative W868Y mutation resulted in a three-fold loss in binding affinity, indicating that the interaction between the aromatic residue and K4me3 depends on the type of aromatic ring.

Comparison with Other PHD Fingers: A Negative Charge and a Structural Swap in the K4me3 Pocket

The core of the PHD finger and the three-stranded β sheet organization of the complex is well conserved in the crystal structures of the BPTF-, RAG2-, and ING2-H3K4me3 complexes and the solution structure of the TAF3 complex (Figure S5). Differences are restricted to the L1 and L2 loops and the β1-β2 turn, which have the highest sequence diversity and have different lengths in the three sequences. Focusing on the closely related TAF3-, BPTF-, and ING2-PHD fingers, we find that most of the intermolecular interactions are conserved. Striking differences in the interface are the presence of negatively charged D877 and the second aromatic residue W868 in the TAF3-K4me3 pocket (Figure 4). Interestingly, the importance of the electrostatic interaction between D877 and K4me3 might be limited, since alanine substitution of the neutral S222 in ING2, corresponding to TAF3-D877, also resulted in a 16-fold reduction in affinity for H3K4me3 (Pena et al., 2006). In both cases, this loss of affinity is likely due to loss of the intermolecular hydrogen bond with T6. Rather, the presence of two tryptophans might be of more importance for the TAF3-H3K4me3 interaction. Previously, residue I869 was predicted to be part of the K4me3 pocket at the position corresponding to residues

Table 2. Specificity of the TAF3-PHD Finger for H3K4me3 versus H3R2me2a/K4me3

TAF3-PHD[a]	H3K4me3, K_D (μM)	H3R2me2a/K4me3, K_D (μM)	Ratio R2K4/K4[b]
WT	0.31 ± 0.09	2.5 ± 0.2	8.1
W868Y	0.9 ± 0.2		
D877A	4.9 ± 0.2		
D886A	9.0 ± 0.6	4 ± 2 (·10[1])	4.3
D889A	1.7 ± 0.3	3.6 ± 0.4	2.1
D889S	0.63 ± 0.07	2.6 ± 0.2	4.2
BPTF	3.6 ± 0.8	9.4 ± 0.3	2.6

All affinities were determined by using tryptophan fluorescence binding experiments. Average values and their standard deviations are reported when duplicate measurements are available.

[a] Variant of the TAF3-PHD finger, either wild-type (WT) or the indicated mutant.

[b] Ratio R2K4/K4 = $K_{D,H3R2me2a/K4me3}/K_{D,H3K4me3}$.

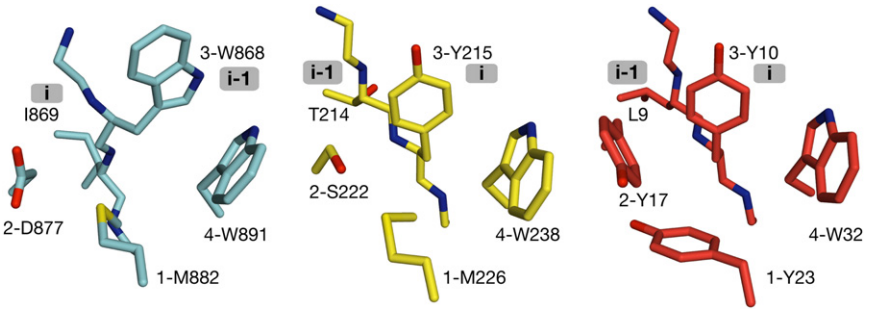

Figure 4. Comparison of the K4me3-Binding Pockets of the TAF3-, ING2-, and BPTF-PHD Fingers

Numbers 1–4 indicate the four positions in the pocket. The relative positions in sequence space of residues W868 and I869 and their corresponding residues in ING2 and BPTF are indicated to emphasize their swap in the TAF3 pocket.

Y215 of ING2 and Y10 of BPTF (Ruthenburg et al., 2007; Vermeulen et al., 2007). This would have resulted in an unprecedented trimethyl-lysine-binding pocket with only a single aromatic amino acid, W891. However, our NOE data unambiguously indicate that I869 is packed against Y857 and P876, away from the K4me3 pocket, whereas we observed intermolecular NOEs between W868 and the K4me3 methyl groups (cf. Figure 2D). Residue I869 should thus be considered as an insertion in the TAF3 amino acid sequence. Interestingly, the adjustment of the local conformation necessary to accommodate W868 in the K4me3 pocket results in an orientation of the inserted I869 equivalent to that of T214 in ING2 and L9 in BPTF (Figure 4). Thus, judged from their order in sequence space, W868 and I869 have swapped their structural roles compared to the corresponding residues in the ING2 and BPTF pockets, underscoring the requirement for two aromatic residues in the K4me3 pocket.

Interaction with H3K4me2

Mono-, di-, and trimethylated histone lysine residues are differently distributed over the genome and are believed to each have a distinct functional outcome, mediated by methylation-state-specific reader proteins (Sims and Reinberg, 2006; Barski et al., 2007; Heintzman et al., 2007). Although it has been firmly established that the TAF3-PHD finger binds preferentially to H3K4me3 (Vermeulen et al., 2007), an earlier report reasoned that the possibility for a hydrogen bond between the remaining amino proton of H3K4me2 and residue D877 would result in the selective binding of dimethylated K4 (Ruthenburg et al., 2007). Here, we studied the interaction of the TAF3-PHD finger with an H3K4me2 peptide by NMR. Consistent with previously reported results (Vermeulen et al., 2007), we find a K_D of 1.4 ± 0.5 μM (data not shown) for the H3K4me2 complex, an ~5-fold lower affinity than for H3K4me3. The high degree of similarity between the ^{1}H-^{15}N HSQC spectra of the two complexes strongly suggests that the structures of the two complexes are nearly identical (Figure 5A). Line-shape analysis indicates that the lifetime of the dimethyl complex is roughly four-fold shorter than that of the trimethyl complex, which is in accordance with destabilization of the complex (Figure S6). In addition, neither D877, nor its neighbors show significant changes in their chemical shifts between the dimethylated and trimethylated H3K4 complex. Significant chemical-shift differences are limited to the backbone and side chain chemical shifts of W868 and W891. Interestingly, their shifts in the dimethyl complex seem to be slightly closer to the unbound values compared to the trimethyl complex (Figure 5B), consistent with studies in model peptides (Hughes et al., 2007a). Together, this argues against the involvement of D877 in hydrogen-bond formation but suggests that the lower affinity for H3K4me2 is due to a weaker interaction with W868 and W891.

Crosstalk by R2 Dimethylation

A central idea in the histone code hypothesis is the occurrence of crosstalk between histone modifications (Fischle et al., 2003). Previously, additional asymmetric dimethylation of R2 (H3R2me2a) was shown to strongly reduce the binding affinity of the TAF3-PHD finger to H3K4me3, whereas only a limited effect was observed for the ING2- or BPTF-PHD fingers (Vermeulen et al., 2007). Interestingly, the H3R2me2a mark has been shown to anticorrelate with gene activity (Guccione et al., 2006). Here, we sought to determine the influence of R2 asymmetric dimethylation on the TAF3-PHD:H3K4me3 interaction.

The binding affinity of the TAF3-PHD finger for a doubly modified peptide (H3R2me2a/K4me3) was 2.5 ± 0.2 μM, as determined with tryptophan fluorescence (Table 2), which is roughly eight-fold reduced compared to the H3K4me3 peptide. In contrast, we measured only a two- to three-fold decrease in affinity for the BPTF-PHD finger (Table 2). Line-shape analysis of the NMR spectra confirms that the strong loss of affinity for TAF3 corresponds to a destabilization of the doubly modified complex (Figure S6). Chemical-shift comparison between the H3K4me3 complex and the H3R2me2a/K4me3 complex shows considerable differences for residues in the R2 pocket (G884, C885, D886, and D889) and several residues in the L2 loop facing R2 (E906, Q908, and W909) (Figure 5A). Interestingly, the backbone resonances of D886 and D889 are shifted toward their free-state position, whereas the resonance of G884 is shifted toward a completely new position, suggesting a reorientation of the R2me2a side chain (Figure 5C). Mutational analysis implies that the R2me2a side chain is too bulky to fit in the R2 pocket. Table 2 lists the binding affinity for both the singly modified H3K4me3 and the doubly modified H3R2me2a/K4me3 peptide of mutant proteins in which key residues, D886 and D889, were replaced with smaller amino acids. As expected, these mutants have a lower affinity for the singly modified peptide, since the electrostatic interaction with R2 is lost. However, additional asymmetric dimethylation of R2 reduces affinity by only a factor of two to four for the mutant proteins, compared to the eight-fold reduction for the wild-type protein. Thus, mutants with a wider R2 pocket are less affected by R2 methylation, resulting in a relative gain in affinity.

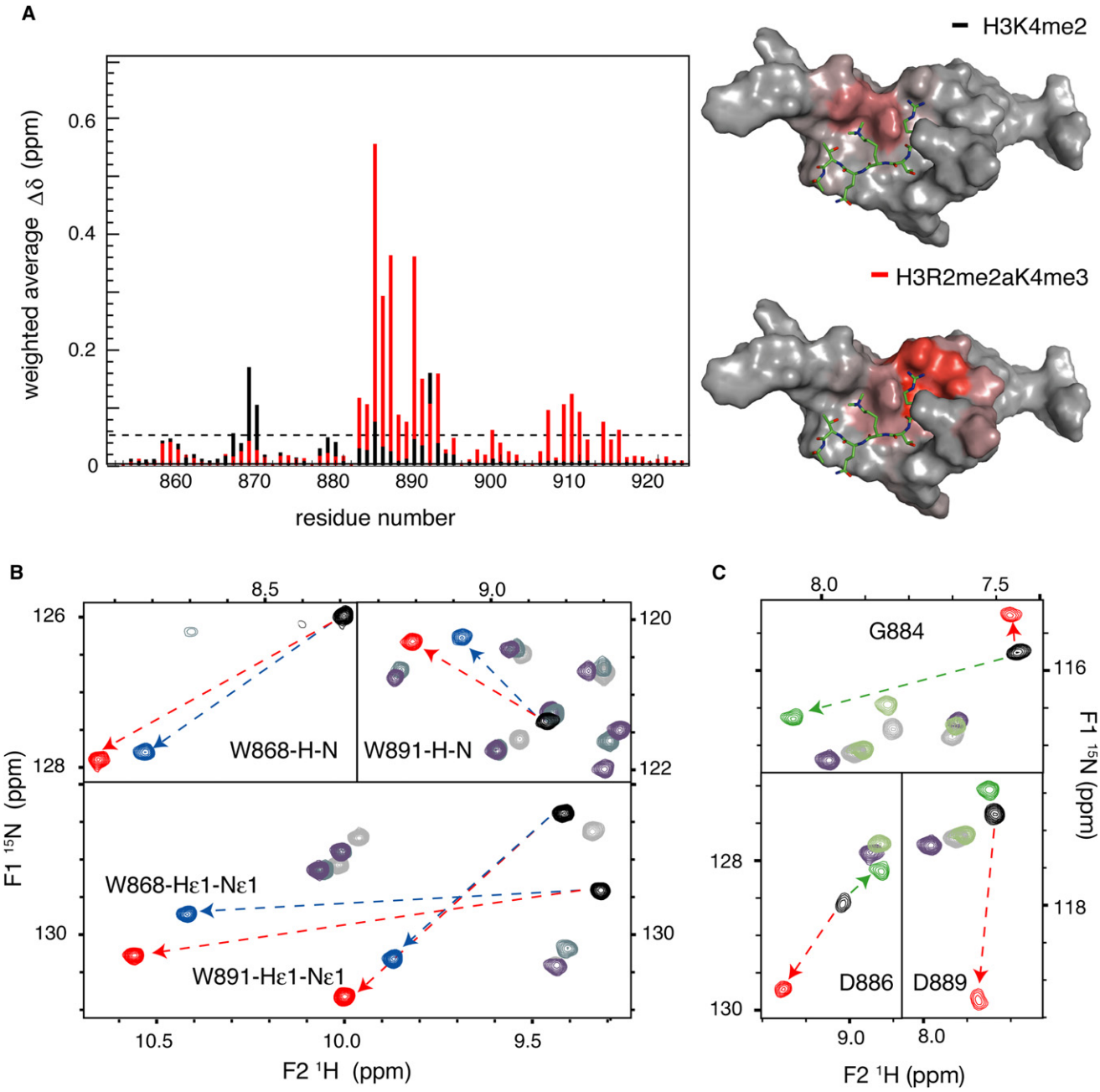

Figure 5. Interaction of the TAF3-PHD Finger with H3K4me2 and H3R2me2a/K4me3 Peptides

(A) Chemical-shift comparison between the H3K4me3-bound PHD finger and the H3K4me2 (black) or the H3R2me2a/K4me3 complex (red) based on ^{1}H-^{15}N HSQC spectra. Surface plots of the TAF3-PHD:H3K4me3 complex are shown on the right, colored from gray ($\Delta\delta = 0$) to red ($\Delta\delta = 0.5$).

(B and C) Sections from the ^{1}H-^{15}N HSQC of the free TAF3-PHD finger (black/gray), the H3K4me3 complex (red/purple), and (B), the H3K4me2 complex (blue/dark blue) and (C) the H3R2me2a/K4me3 complex (green/dark green). Resonances belonging to W868, W891, G884, D886, and D889 are indicated.

DISCUSSION

In this study, we have determined the solution structures of the PHD finger of the TAF3 subunit of the basal transcription factor TFIID, both free and in complex with H3K4me3. Affinity measurements, mutagenesis, and NMR titration experiments provided detailed insight into the methylation-state specificity of the TAF3-PHD:H3K4me3 interaction and the crosstalk by adjacent dimethylation of H3R2.

A Structural Swap in the K4me3-Binding Pocket Underscores the Requirement for Cation-π Interactions by Two Aromatic Residues

The K4me3-binding pocket of the TAF3-PHD finger contains two aromatic residues, similar to other PHD and Royal domains that bind H3K4me3. However, the conserved insertion of I869 necessitates a rearrangement of the local structure to allow W868 in the binding pocket, thus swapping the structural roles of

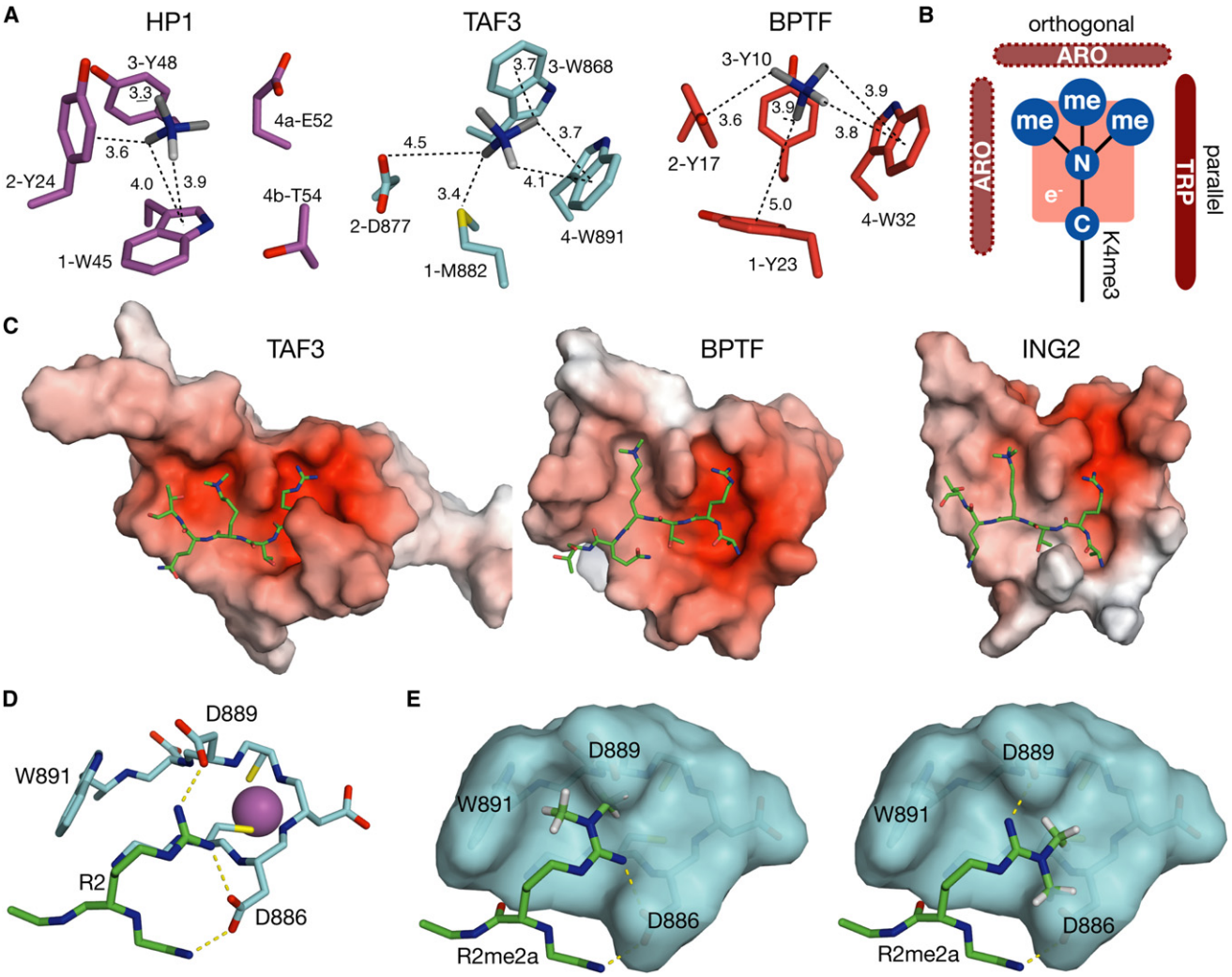

Figure 6. Cation-π Interactions in the K4me3-Binding Pocket, Electrostatic Potential of the Interaction Surface, and Structural Basis of Crosstalk by Adjacent R2 Dimethylation

(A) Comparison of the trimethyl-lysine pockets of the chromodomain of HP1 and the PHD domains of TAF3 and BPTF. Distances from the methyl carbon and the Cε carbon (light gray) of the Kme3 to the surrounding residues are indicated.

(B) Model of trimethyl-lysine recognition emphasizing the importance of a tryptophan parallel to the extended lysine side chain. A second aromatic residue (dashed) is usually orthogonal to this side chain, but can also be in a parallel position. A third electron-rich residue forms the floor of the pocket, whereas a fourth residue is not required.

(C) Electrostatic potential at the solvent-accessible surface projected on the van derWaals surface of the PHD domains of TAF3, BPTF, and ING2. Red denotes areas of negative potential. Potentials were calculated by using the APBS (Baker et al., 2001) plug in of PyMOL (DeLano Scientific LLC, 2008) with the AMBER force field.

(D) Model of the local structure in the R2 pocket showing intermolecular hydrogen bonds between R2 and D886 and D889.

(E) Models of the asymmetrically dimethylated R2 (R2me2a) side chain in the R2 pocket (van derWaals surface shown) based on the model in (D). The additional methyl groups are shown, including their protons; other protons are omitted for clarity.

residues I869 and W868 compared to their counterparts in the BPTF- or ING2-PHD domains. The apparent requirement for two aromatic residues and the close proximity of their electron-rich π-ring systems and the positively charged K4me3 are suggestive of favorable cation-π interactions (Dougherty, 1996; Gallivan and Dougherty, 1999; Minoux and Chipot, 1999). Distances between the aromatic rings of W868 and W891 and the Cε atom or the methyl carbons of K4 are on the order of a van derWaals contact (3.5–4 Å) and are similar to distances found in other trimethyl-lysine complexes (Figure 6A; Table S3). Moreover, the geometry is similar to that found for the complex of H3K9me3 and the chromodomain of protein HP1, for which the presence of a cation-π interaction was recently demonstrated experimentally (Hughes et al., 2007b). In addition, aromatic chemical shifts of W868 and W891 are significantly more strongly perturbed upon complex formation than W894 and W909, which are also part of the interface (Figure S7). Also, the ^{1}H shifts of the K4 methyl groups are strongly shifted upfield

upon complex formation. Intriguingly, there is rapid rotation around the Cε-Nζ bond, creating a single averaged chemical environment for all three methyl groups.

Examination of different trimethyl-lysine pockets of Royal and PHD domains reveals that, in all cases, one of the two required aromatic residues is a tryptophan in a parallel orientation to the extended trimethyl-lysine side chain (Figure 6B; Table S4). A tryptophan in this position is ideally suited to create a deep pocket for the long lysine side chain. Additionally, its large electric quadrupole moment results in stronger cation-π interactions than those involving tyrosine or phenylalanine (Dougherty, 1996), thereby anchoring the trimethyl-lysine side chain by interactions with the Cε and the methyl carbons. The second aromatic residue mostly interacts with the methyl groups from an orthogonal orientation. The only exception so far is the RAG2-PHD finger, in which the two aromatic residues are in a parallel orientation (Ramon-Maiques et al., 2007). The two aromatic residues are complemented by a third electron-rich residue, either an aromatic residue or methionine. A fourth or fifth residue in the K4me3 pocket is not required, resulting in half-open (TAF3 and ING2 [Pena et al., 2006]) or channel-like pockets (RAG2 [Ramon-Maiques et al., 2007]).

Structural Basis of Affinity

The binding affinity of the TAF3-PHD finger for H3K4me3 (K_D = 0.31 μM) is among the highest reported thus far. Although one should be careful in comparing binding affinities determined by using different methodologies, reported K_Ds for other PHD domains are at least five- to ten-fold higher, ranging from 2 to 4 μM (ING2 and BPTF [Li et al., 2006; Pena et al., 2006; this study]) to ~30 μM (RAG2 [Ramon-Maiques et al., 2007]). Binding affinities of the Royal domains also fall in this range, although the tandem Tudor domain of JMJD2a was recently reported to bind H3K4me3 with a K_D of 0.5 μM, compared to a K_D of ~10 μM reported earlier (Huang et al., 2006; Lee et al., 2008).

Several factors contribute to the enhanced H3K4me3 affinity of the TAF3-PHD finger. First, mutant W868Y was three-fold less effective in H3K4me3 binding, indicating that the additional tryptophan in the K4me3-binding pocket generates stronger cation-π interactions than the corresponding tyrosine in ING2 or BPTF. Second, although there are no large differences in the total buried surface area, residue A1 and the N terminus are buried more deeply in the TAF3 complex (Figure 6C). Finally, the TAF3-PHD finger has several negatively charged residues in the R2- and K4me3-binding pockets and in the L2 loop, resulting in a more pronounced negative electrostatic surface potential than for the ING2- or BPTF-PHD domain (Figure 6C). Such a network of electrostatic interactions might result in a significant stabilization of the H3K4me3 complex.

Discrimination of the H3K4 Methylation State

Nonmethylated or mono-methylated forms of H3K4 do not interact with the TAF3-PHD finger or other H3K4me3-binding PHD and Royal domains. However, these domains bind dimethylated H3K4 with only a two- to ten-fold lower affinity than H3K4me3 (Jacobs and Khorasanizadeh, 2002; Li et al., 2006; Pena et al., 2006; Taverna et al., 2006; Vermeulen et al., 2007). Likely, this reflects that two methyl groups are sufficient to generate a strong interaction with the two conserved aromatic residues in the K4me3-binding pocket (Figure 6B; Table S3). It was expected that the presence of the hydrogen-bond acceptor D877 in the TAF3-K4me3-binding pocket would alter this methylation-state specificity (Ruthenburg et al., 2007), as hydrogen-bond formation is used in PHD domains that specifically bind to nonmethylated H3K4 (Lan et al., 2007; Ooi et al., 2007) or dimethylated H3K4 (Botuyan et al., 2006). However, we find that the five-fold lower affinity of the TAF3-PHD domain for H3K4me2 is most likely caused by weaker interactions with W868/W891. As chemical-shift comparison indicates that the two complexes are structurally very similar, we suggest that D877 is simply too far away from the amine group to allow for efficient hydrogen bonding. Thus, both in the H3K4me3 and H3K4me2 complex, the electrostatic interaction between D877 and K4me2/3 is weaker than the cation-π interaction with W868/W891, as the trimethylated amino group is in van derWaals range with the aromatic rings, but not with the carboxylate group. We predict that substitution by a glutamic acid, by virtue of its longer side chain, will result in hydrogen-bond formation and, consequently, a modest specificity for H3K4me2, as was recently shown for BPTF (Li et al., 2007).

Structural Basis for Crosstalk by R2 Dimethylation

Affinity measurements and spectroscopic data show that asymmetric dimethylation of H3R2 interferes with the ability of the TAF3-PHD finger to bind to H3K4me3, consistent with earlier results (Vermeulen et al., 2007). The structural interpretation of the approximately eight-fold reduction in binding affinity is complicated by the poor definition of the position of the R2 guanidinium group in the TAF3-H3K4me3 ensemble of structures. Although direct spectroscopic evidence is absent, chemical-shift perturbation of residues D886 and D889 in the R2-binding pocket; their contribution to binding affinity, as shown by mutation analysis; and their strict conservation strongly suggest their involvement in an intermolecular interaction with R2 in the H3K4me3 complex, which appears to be absent in the H3R2me2a/K4me3 complex. Therefore, we created a model of the R2-binding pocket by defining ambiguous interaction restraints between H3R2 and D886/D889 and neighboring residues by using the docking program HADDOCK (Dominguez et al., 2003; de Vries et al., 2007). The model shows that the R2 guanidinium group is hydrogen bonded to the carboxyl groups of D889 and D886 (Figure 6D), similar to the R2 pockets in the crystal structures of the BPTF- and ING2-PHD domains (Li et al., 2006; Pena et al., 2006). These intermolecular hydrogen bonds are probably of moderate strength, as the guanidinium protons could not be observed in the NMR spectra, pointing to extensive exchange line broadening caused by rotation around the Cζ-Nη and Nε-Cζ bonds (Henry and Sykes, 1995). The model suggests that asymmetric dimethylation of H3R2 is incompatible with these intermolecular hydrogen bonds, in accordance with the observed loss in binding affinity (Figure 6E). Furthermore, without reorientation of the R2me2a side chain severe atomic clashes would result, consistent with chemical-shift and mutation data. By comparison, the R2 pocket in the BPTF-PHD finger seems able to accommodate R2me2a without significant disruption of hydrogen bonds (data not shown), consistent with the small effect on binding affinity by R2me2a modification. The RAG2-PHD finger has a slightly increased affinity for the doubly modified H3 tail, due to interaction

between R2me2a and a tyrosine at the position corresponding to TAF3-G884 (Ramon-Maiques et al., 2007).

The interference with the TAF3-H3K4me3 interaction by asymmetric dimethylation of H3R2 shown by these in vitro experiments point to the presence of a R2/K4 "methyl-methyl" switch in the histone code (Fischle et al., 2003). Such interference effects can provide a dynamic regulation mechanism as observed for the H3K9/S10 "phospho-methyl" switch (Fischle et al., 2003). Recently, asymmetric dimethylation of H3R2 has been linked to gene repression and was shown to prevent trimethylation of H3K4 (Guccione et al., 2007; Kirmizis et al., 2007). Recruitment of the H3R2 methyltransferase PRMT6 to gene loci was shown to result in enhanced H3R2me2a modification and in reduced gene expression (Hyllus et al., 2007). Whereas it was shown that the H3R2me2a modification directly inhibits H3K4 trimethylation by the MLL methyltransferase (Guccione et al., 2007; Hyllus et al., 2007), our experiments indicate that H3R2me2a modification directly interferes with the TAF3-H3K4me3 interaction. Similarly, binding to H3K4me3 peptides by the PHD finger of the Spp1p subunit of the Set1/COMPASS histone methyltransferase complex is also sensitive to concurrent H3R2me2a modification (Kirmizis et al., 2007). Such crosstalk would provide a fail-safe mechanism to rapidly dissociate TFIID from certain promoters by a R2/K4 "methyl-methyl" switch, which would be analogous to the "methyl-phospho" switch model proposed for the HP1 protein (Fischle et al., 2003). Future experiments establishing the co-occurrence of the R2me2a and K4me3 marks on promoters are required to test this model.

EXPERIMENTAL PROCEDURES

Protein Expression and Purification

A single colony from freshly transformed BL21-DE3 cells with the corresponding GST-PHD(mutant) construct was grown overnight and adapted to Luria broth (LB) or minimal medium (MM), both supplemented with 50 μg/ml ampicilin. A 50-fold diluted fraction was grown to an OD_{600} of 0.7, supplemented with 0.4 mM IPTG, and grown for another 2 hr (3 hr for MM). Cells were lysed in 50 ml ice-cold lysis buffer per liter of culture (50 mM Tris-HCl [pH 8.0], 20% sucrose, 300 mM KCl, 0.1% Triton X-100, 1 mM DTT, and protease inhibitors). After the addition of lysozyme to 0.25 mg/ml and three freeze-thaw cycles, the lysate was subjected to sonification and was cleared by centrifugation at 4°C. Supernatant was loaded on a GA-agarose column (Sigma), washed with lysis and wash buffers (50 mM KH_2PO_4/K_2HPO_4 [pH 7.0], 100 mM KCl, 10 μM $ZnCl_2$, 1 mM DTT, and protease inhibitors), and eluted with 50 mM reduced glutathione in wash buffer. After thrombin digestion (Sigma) at 1 U/mg protein for 2 hr at 37°C, thrombin was inactivated by adding PMSF to 0.5 mM, bound to benzamidine-Sepharose 6B (GE-Healthcare), and removed by filtration. After concentration, the sample was loaded onto a Sephadex-75 (HiLoad 16/60 or 26/60) gel-filtration column, equilibrated with buffer A (20 mM KH_2PO_4/K_2HPO_4 [pH 7.0], 150 mM KCl, 10 μM $ZnCl_2$, 1 mM DTT, and leupeptin and aprotinin at 0.1 μg/ml) with 150 mM KCl. The resulting PHD protein (residues 857–924 of *Mus musculus* TAF3 with a 6 residue N-terminal extension remaining from the thrombin cleavage site) was diluted to buffer A plus 100 mM KCl and was subsequently applied to a MonoQ HR5/5 or MonoQ HR10/10 column equilibrated in this buffer and developed by using a linear gradient from 100 to 1000 mM KCl in buffer A.

Peptide Synthesis

The peptides (residues 1–13 of *Homo sapiens* H3, carboxyamide form) were assembled on an automatic ABI 433A Peptide Synthesizer by using the ABI FastMoc 0.25 mmol protocols with coupling times of 45 min instead of 20 min. Fmoc (9-fluorenylmethoxycarbonyl) amino acid derivatives, activated in situ by using HBTU/HOBt and DiPEA in NMP, were used in coupling steps. Fmoc-ADMA(Pbf)-OH (Novabiochem), Fmoc-Lys$(Me)_2$-OH·HCl (Bachem), and Fmoc-Lys$(Me)_3$-OH·chloride (Bachem) were used to incorporate the asymmetric dimethylarginine (ADMA) and the di- or trimethylated lysine, respectively. The peptides were deprotected and cleaved from the resin by treatment with 25 ml TFA/H_2O/TIS (95:2.5:2.5) for 2 hr at room temperature. Finally, the peptides were precipitated in a MTBE/n-hexane (1/1, v/v) solution. After this, the pellets were dissolved in *tert*.-BuOH/water (1/1, v/v) (ca. 60 ml) and lyophilized to obtain the crude peptides as white, fluffy solids. Every peptide was purified by preparative HPLC. Peptides were characterized by HPLC (H3K4me3, 98%; H3K4me2, 100%; H3R2me2a/K4me3, 99%) and by ESI-MS (exp./calc. mass: H3K4me3, 1403.96/1403.83; H3K4me2, 1388.92/1388.81; H3R2me2a/K4me3, 1431.92/1431.86).

Tryptophan Fluorescence Binding Experiments

The TAF3-PHD finger was diluted in H3-binding buffer (20 mM Tris-HCl [pH 8.0], 150 mM KCl, 1 mM DTT, 10 μM $ZnCl_2$, 0.001% Tween-20) to 100–200 nM for K_Ds below or equal to 1 μM and to 1 μM for K_Ds above 1 μM. Tryptophan fluorescence was determined by using a Varian Cary Eclipse fluorescence spectrophotometer with 1.2 ml cuvettes with stirring, a 280 nm excitation wavelength, and a 2.5 nm slit width. Emission was determined in the range of 335–355 nm with a 10 nm (for 100–200 nM PHD) or a 2.5 nm slit width (for 1 μM PHD) with an averaging time of 5 s and a 2 nm data interval. Each measurement was repeated at least twice.

NMR Spectroscopy and Data Analysis

NMR samples contained 0.2 mM (free) or 0.4 mM (complex) uniformly ^{13}C,^{15}N-labeled PHD domain and unlabeled H3K4me3 peptide in a 1:1 ratio (complex), 150 mM KCl, 20 mM KH_2PO_4/K_2HPO_4 (pH 7), and 10 μM $ZnCl_2$. All NMR experiments were performed on Bruker Avance II spectrometers at field strengths corresponding to 600, 700, 750, or 900 MHz proton resonance frequency at 20°C. Spectra were processed by using NMRPipe (Delaglio et al., 1995) and were analyzed by using Sparky (http://www.cgl.ucsf.edu/home/sparky/). Backbone and side chain resonances of the TAF3-PHD finger were assigned by using 3D HNCAHA, CBCACONH, HNCACB, HNCO, HNCACO, H(C)CH-TOCSY, (H)CCH-TOCSY; 2D ^{15}N-filtered NOESY; and 2D C_β-H_δ and C_β-H_ε correlation spectra, by employing the program MARS for automatic backbone assignment (Jung and Zweckstetter, 2004) and the in-house-developed program PROSIAS for automated assignment of the aliphatic side chain resonances. Assignments of the free PHD domain could be transferred to the bound state by using additional 3D HNCA, HNCAHA, CBCACONH, and NOESY spectra of the bound PHD domain. The protonation state of the Zn-coordinating H893 side chain was set to $N_{\varepsilon 2}$ based on the observed NOESY crosspeaks. The sequential-assignment approach (Wüthrich, 1986) was used to assign the bound H3K4me3 peptide, relying on 2D $^{13}C/^{15}N$-filtered NOESY (mixing time of 150 ms) and TOCSY (mixing time 20-60 ms) experiments (Zwahlen et al., 1997). These were recorded at 10, 15, and 20°C in order to resolve overlap and to verify assignments. Assignments of TAF3 in the H3K4me3 complex could easily be transferred to the H3K4me2 and H3R2me2a/K4me3 complex by using the titration data. The chemical-shift perturbation of residue *i*, $\Delta\delta_i$, was calculated as

$$\Delta\delta_i = \sqrt{\sum_A \left(\frac{\delta_{bound,A} - \delta_{free,A}}{\sigma_A}\right)^2},$$

where σ_A is the standard deviation in the chemical shift of atom *A*, as reported in the BMRB database (Ulrich et al., 2008). Distance restraints for structure calculations were obtained from 2D NOESY and 3D ^{15}N- and ^{13}C-separated NOESY experiments by using a mixing time of 100 ms. Intermolecular NOEs were derived from a 2D $^1H,^1H$ ^{13}C-edited-filtered NOESY and from comparison of 2D F1,F2 and F2 $^{15}N,^{13}C$-filtered NOESYs with a 150 ms mixing time.

Structure Calculation and Validation

The NOE crosspeaks from the 2D NOESY and 3D ^{15}N- and ^{13}C-separated NOESYs were assigned and converted into distance restraints by using CYANA 2.1 (Guntert et al., 1997; Herrmann et al., 2002). Crosspeaks from the 2D F2 $^{15}N,^{13}C$-filtered NOESY were assigned and converted into distance constraints manually. Dihedral angle restraints for the ϕ,ψ angles of the PHD domain/H3 were derived from N, C′, C_α, H_α, and C_β/H_N and H_α chemical shifts

by using TALOS/CSI 2.2 (Cornilescu et al., 1999; Wishart and Sykes, 1994). Tetrahedral zinc coordination was enforced by using restraints between the coordinating atoms and the Zn ion (Simonson and Calimet, 2002). First, 10 ensembles of 50 structures were calculated by using CYANA. For each ensemble, the ten best structures were used to produce a distance restraint lists. From the list with the fewest total restraints, only the restraints that were reproduced in all other nine lists were retained to produce a final restraint list. This final list was then used to calculate 100 structures in CNS (Brunger et al., 1998), which were subsequently refined in explicit water by using the RECOORD protocol (Nederveen et al., 2005). The final ensemble contained the 20 lowest-energy structures, contained neither distance violations > 0.5 Å, nor dihedral angle violation > 5°, and was validated by using PROCHECK and WHATCHECK (Hooft et al., 1996; Laskowski et al., 1996). The CYANA library and CNS topology and parameter files were extended to include the trimethyl-lysine residue. Partial charges were assigned based on studies on tetramethylammonium (Patra et al., 2007). To mimic the electrostatic component of the cation-π interaction during water refinement, small partial charges were assigned to the aromatic ring atoms (Minoux and Chipot, 1999; Felder et al., 2001).

ACCESSION NUMBERS

Coordinates for the free and H3K4me3-bound TAF3-PHD finger have been deposited in the RCSB Protein Data Bank with accession codes 2k16 and 2k17, respectively. The chemical shift assignments have been deposited in the BioMagResBank database with accession codes 15670 and 15671, respectively.

SUPPLEMENTAL DATA

Supplemental data include three tables and seven figures and can be found with this article online at http://www.structure.org/cgi/content/full/16/8/1245/DC1/.

ACKNOWLEDGMENTS

We gratefully acknowledge Davidson and Patel for providing plasmids. We thank members of the R.B./Kaptein lab and the H.M.T. lab for useful suggestions and for stimulating discussions. We also thank Klaas Mulder and Florence Mouson for critical reading of the manuscript. This work was supported by grants to the H.M.T. lab from the European Union (STREP LSHG-CT-2004-502950) and the Netherlands Proteomics Centre. This work was supported by European Commission funding through the SPINE2-COMPLEXES project LSHG-CT-2006-031220.

Received: March 7, 2008
Revised: April 26, 2008
Accepted: April 28, 2008
Published: August 5, 2008

REFERENCES

Baker, N.A., Sept, D., Joseph, S., Holst, M.J., and McCammon, J.A. (2001). Electrostatics of nanosystems: application to microtubules and the ribosome. Proc. Natl. Acad. Sci. USA *98*, 10037–10041.

Barski, A., Cuddapah, S., Cui, K.R., Roh, T.Y., Schones, D.E., Wang, Z.B., Wei, G., Chepelev, I., and Zhao, K.J. (2007). High-resolution profiling of histone methylations in the human genome. Cell *129*, 823–837.

Bienz, M. (2006). The PHD finger, a nuclear protein-interaction domain. Trends Biochem. Sci. *31*, 35–40.

Botuyan, M.V., Lee, J., Ward, I.M., Kim, J.E., Thompson, J.R., Chen, J.J., and Mer, G. (2006). Structural basis for the methylation state-specific recognition of histone H4–K20 by 53BP1 and Crb2 in DNA repair. Cell *127*, 1361–1373.

Brunger, A.T., Adams, P.D., Clore, G.M., DeLano, W.L., Gros, P., Grosse-Kunstleve, R.W., Jiang, J.S., Kuszewski, J., Nilges, M., Pannu, N.S., et al. (1998). Crystallography & NMR system: a new software suite for macromolecular structure determination. Acta Crystallogr. D Biol. Crystallogr. *54*, 905–921.

Cornilescu, G., Delaglio, F., and Bax, A. (1999). Protein backbone angle restraints from searching a database for chemical shift and sequence homology. J. Biomol. NMR *13*, 289–302.

de Vries, S.J., van Dijk, A.D., Krzeminski, M., van Dijk, M., Thureau, A., Hsu, V., Wassenaar, T., and Bonvin, A.M. (2007). HADDOCK versus HADDOCK: new features and performance of HADDOCK2.0 on the CAPRI targets. Proteins *69*, 726–733.

Delaglio, F., Grzesiek, S., Vuister, G.W., Zhu, G., Pfeifer, J., and Bax, A. (1995). NMRPipe: a multidimensional spectral processing system based on UNIX pipes. J. Biomol. NMR *6*, 277–293.

DeLano Scientific LLC (2008). PyMOL (http://www.pymol.org).

Dominguez, C., Boelens, R., and Bonvin, A.M. (2003). HADDOCK: a protein-protein docking approach based on biochemical or biophysical information. J. Am. Chem. Soc. *125*, 1731–1737.

Dougherty, D.A. (1996). Cation-π interactions in chemistry and biology: a new view of benzene, Phe, Tyr, and Trp. Science *271*, 163–168.

Felder, C., Jiang, H.L., Zhu, W.L., Chen, K.X., Silman, I., Botti, S.A., and Sussman, J.L. (2001). Quantum/classical mechanical comparison of cation-π interactions between tetramethylammonium and benzene. J. Phys. Chem. A *105*, 1326–1333.

Fischle, W., Wang, Y.M., and Allis, C.D. (2003). Binary switches and modification cassettes in histone biology and beyond. Nature *425*, 475–479.

Flanagan, J.F., Mi, L.Z., Chruszcz, M., Cymborowski, M., Clines, K.L., Kim, Y.C., Minor, W., Rastinejad, F., and Khorasanizadeh, S. (2005). Double chromodomains cooperate to recognize the methylated histone H3 tail. Nature *438*, 1181–1185.

Gallivan, J.P., and Dougherty, D.A. (1999). Cation-π interactions in structural biology. Proc. Natl. Acad. Sci. USA *96*, 9459–9464.

Guccione, E., Martinato, F., Finocchiaro, G., Luzi, L., Tizzoni, L., Dall' Olio, V., Zardo, G., Nervi, C., Bernard, L., and Amati, B. (2006). Myc-binding-site recognition in the human genome is determined by chromatin context. Nat. Cell Biol. *8*, 764–770.

Guccione, E., Bassi, C., Casadio, F., Martinato, F., Cesaroni, M., Schuchlautz, H., Luscher, B., and Amati, B. (2007). Methylation of histone H3R2 by PRMT6 and H3K4 by an MLL complex are mutually exclusive. Nature *449*, 933–937.

Guenther, M.G., Levine, S.S., Boyer, L.A., Jaenisch, R., and Young, R.A. (2007). A chromatin landmark and transcription initiation at most promoters in human cells. Cell *130*, 77–88.

Guntert, P., Mumenthaler, C., and Wuthrich, K. (1997). Torsion angle dynamics for NMR structure calculation with the new program DYANA. J. Mol. Biol. *273*, 283–298.

Heintzman, N.D., Stuart, R.K., Hon, G., Fu, Y., Ching, C.W., Hawkins, R.D., Barrera, L.O., Van Calcar, S., Qu, C., Ching, K.A., et al. (2007). Distinct and predictive chromatin signatures of transcriptional promoters and enhancers in the human genome. Nat. Genet. *39*, 311–318.

Henry, G.D., and Sykes, B.D. (1995). Determination of the rotational-dynamics and pH-dependence of the hydrogen-exchange rates of the arginine guanidino group using Nmr-spectroscopy. J. Biomol. NMR *6*, 59–66.

Herrmann, T., Guntert, P., and Wuthrich, K. (2002). Protein NMR structure determination with automated NOE assignment using the new software CANDID and the torsion angle dynamics algorithm DYANA. J. Mol. Biol. *319*, 209–227.

Hooft, R.W., Vriend, G., Sander, C., and Abola, E.E. (1996). Errors in protein structures. Nature *381*, 272.

Huang, Y., Fang, J., Bedford, M.T., Zhang, Y., and Xu, R.M. (2006). Recognition of histone H3 lysine-4 methylation by the double tudor domain of JMJD2A. Science *312*, 748–751.

Hughes, R.M., Benshoff, M.L., and Waters, M.L. (2007a). Effects of chain length and N-methylation on a cation-π interaction in a β-hairpin peptide. Chemistry (Easton) *13*, 5753–5764.

Hughes, R.M., Wiggins, K.R., Khorasanizadeh, S., and Waters, M.L. (2007b). Recognition of trimethyllysine by a chromodomain is not driven by the hydrophobic effect. Proc. Natl. Acad. Sci. USA *104*, 11184–11188.

Hyllus, D., Stein, C., Schnabel, K., Schiltz, E., Imhof, A., Dou, Y., Hsieh, J., and Bauer, U.M. (2007). PRMT6-mediated methylation of R2 in histone H3 antagonizes H3 K4 trimethylation. Genes Dev. *21*, 3369–3380.

Jacobs, S.A., and Khorasanizadeh, S. (2002). Structure of HP1 chromodomain bound to a lysine 9-methylated histone H3 tail. Science *295*, 2080–2083.

Jung, Y.S., and Zweckstetter, M. (2004). Mars–robust automatic backbone assignment of proteins. J. Biomol. NMR *30*, 11–23.

Kirmizis, A., Santos-Rosa, H., Penkett, C.J., Singer, M.A., Vermeulen, M., Mann, M., Bahler, J., Green, R.D., and Kouzarides, T. (2007). Arginine methylation at histone H3R2 controls deposition of H3K4 trimethylation. Nature *449*, 928–932.

Kouzarides, T. (2007). Chromatin modifications and their function. Cell *128*, 693–705.

Lan, F., Collins, R.E., De Cegli, R., Alpatov, R., Horton, J.R., Shi, X.B., Gozani, O., Cheng, X.D., and Shi, Y. (2007). Recognition of unmethylated histone H3 lysine 4 links BHC80 to LSD1-mediated gene repression. Nature *448*, 718–722.

Laskowski, R.A., Rullmannn, J.A., MacArthur, M.W., Kaptein, R., and Thornton, J.M. (1996). AQUA and PROCHECK-NMR: programs for checking the quality of protein structures solved by NMR. J. Biomol. NMR *8*, 477–486.

Lee, J., Thompson, J.R., Botuyan, M.V., and Mer, G. (2008). Distinct binding modes specify the recognition of methylated histones H3K4 and H4K20 by JMJD2A-tudor. Nat. Struct. Mol. Biol. *15*, 109–111.

Li, H., Fischle, W., Wang, W., Duncan, E.M., Liang, L., Murakami-Ishibe, S., Allis, C.D., and Patel, D.J. (2007). Structural basis for lower lysine methylation state-specific readout by MBT repeats of L3MBTL1 and an engineered PHD finger. Mol. Cell *28*, 677–691.

Li, H.T., Ilin, S., Wang, W.K., Duncan, E.M., Wysocka, J., Allis, C.D., and Patel, D.J. (2006). Molecular basis for site-specific read-out of histone H3K4me3 by the BPTF PHD finger of NURF. Nature *442*, 91–95.

Matthews, A.G., Kuo, A.J., Ramon-Maiques, S., Han, S., Champagne, K.S., Ivanov, D., Gallardo, M., Carney, D., Cheung, P., Ciccone, D.N., et al. (2007). RAG2 PHD finger couples histone H3 lysine 4 trimethylation with V(D)J recombination. Nature *450*, 1106–1110.

Minoux, H., and Chipot, C. (1999). Cation-π interactions in proteins: can simple models provide an accurate description? J. Am. Chem. Soc. *121*, 10366–10372.

Nederveen, A.J., Doreleijers, J.F., Vranken, W., Miller, Z., Spronk, C.A., Nabuurs, S.B., Guntert, P., Livny, M., Markley, J.L., Nilges, M., et al. (2005). RECOORD: a recalculated coordinate database of 500+ proteins from the PDB using restraints from the BioMagResBank. Proteins *59*, 662–672.

Ooi, S.K., Qiu, C., Bernstein, E., Li, K.Q., Jia, D., Yang, Z., Erdjument-Bromage, H., Tempst, P., Lin, S.P., Allis, C.D., et al. (2007). DNMT3L connects unmethylated lysine 4 of histone H3 to de novo methylation of DNA. Nature *448*, 714–717.

Pascual, J., Martinez-Yamout, M., Dyson, H.J., and Wright, P.E. (2000). Structure of the PHD zinc finger from human Williams-Beuren syndrome transcription factor. J. Mol. Biol. *304*, 723–729.

Patra, S.M., Bastug, T., and Kuyucak, S. (2007). Binding of organic cations to gramicidin A channel studied with AutoDock and molecular dynamics simulations. J. Phys. Chem. B *111*, 11303–11311.

Pena, P.V., Davrazou, F., Shi, X.B., Walter, K.L., Verkhusha, V.V., Gozani, O., Zhao, R., and Kutateladze, T.G. (2006). Molecular mechanism of histone H3K4me3 recognition by plant homeodomain of ING2. Nature *442*, 100–103.

Ramon-Maiques, S., Kuo, A.J., Carney, D., Matthews, A.G., Oettinger, M.A., Gozani, O., and Yang, W. (2007). The plant homeodomain finger of RAG2 recognizes histone H3 methylated at both lysine-4 and arginine-2. Proc. Natl. Acad. Sci. USA *104*, 18993–18998.

Ruthenburg, A.J., Allis, C.D., and Wysocka, J. (2007). Methylation of lysine 4 on histone H3: intricacy of writing and reading a single epigenetic mark. Mol. Cell *25*, 15–30.

Santos-Rosa, H., Schneider, R., Bannister, A.J., Sherriff, J., Bernstein, B.E., Emre, N.C.T., Schreiber, S.L., Mellor, J., and Kouzarides, T. (2002). Active genes are tri-methylated at K4 of histone H3. Nature *419*, 407–411.

Shi, X., Hong, T., Walter, K.L., Ewalt, M., Michishita, E., Hung, T., Carney, D., Pena, P., Lan, F., Kaadige, M.R., et al. (2006). ING2 PHD domain links histone H3 lysine 4 methylation to active gene repression. Nature *442*, 96–99.

Simonson, T., and Calimet, N. (2002). Cys(x)His(y)-Zn^{2+} interactions: thiol vs. thiolate coordination. Proteins *49*, 37–48.

Sims, R.J., and Reinberg, D. (2006). Histone H3 Lys 4 methylation: caught in a bind? Genes Dev. *20*, 2779–2786.

Sims, R.J., Chen, C.F., Santos-Rosa, H., Kouzarides, T., Patel, S.S., and Reinberg, D. (2005). Human but not yeast CHD1 binds directly and selectively to histone H3 methylated at lysine 4 via its tandem chromodomains. J. Biol. Chem. *280*, 41789–41792.

Strahl, B.D., and Allis, C.D. (2000). The language of covalent histone modifications. Nature *403*, 41–45.

Taverna, S.D., Ilin, S., Rogers, R.S., Tanny, J.C., Lavender, H., Li, H.T., Baker, L., Boyle, J., Blair, L.P., Chait, B.T., et al. (2006). Yng1 PHD finger binding to H3 trimethylated at K4 promotes NuA3 HAT activity at K14 of H3 and transcription at a subset of targeted ORFs. Mol. Cell *24*, 785–796.

Ulrich, E.L., Akutsu, H., Doreleijers, J.F., Harano, Y., Ioannidis, Y.E., Lin, J., Livny, M., Mading, S., Maziuk, D., Miller, Z., et al. (2008). BioMagResBank. Nucleic Acids Res. *36*, D402–D408.

Vermeulen, M., Mulder, K.W., Denissov, S., Pijnappel, W.W., van Schaik, F.M., Varier, R.A., Baltissen, M.P., Stunnenberg, H.G., Mann, M., and Timmers, H.T.M. (2007). Selective anchoring of TFIID to nucleosomes by trimethylation of histone H3 lysine 4. Cell *131*, 58–69.

Wishart, D.S., and Sykes, B.D. (1994). The 13C chemical-shift index: a simple method for the identification of protein secondary structure using 13C chemical-shift data. J. Biomol. NMR *4*, 171–180.

Wüthrich, K. (1986). NMR of Proteins and Nucleic Acids (New York, NY: Wiley).

Wysocka, J., Swigut, T., Xiao, H., Milne, T.A., Kwon, S.Y., Landry, J., Kauer, M., Tackett, A.J., Chait, B.T., Badenhorst, P., et al. (2006). A PHD finger of NURF couples histone H3 lysine 4 trimethylation with chromatin remodelling. Nature *442*, 86–90.

Zwahlen, C., Legault, P., Vincent, S.J.F., Greenblatt, J., Konrat, R., and Kay, L.E. (1997). Methods for measurement of intermolecular NOEs by multinuclear NMR spectroscopy: application to a bacteriophage lambda N-peptide/boxB RNA complex. J. Am. Chem. Soc. *119*, 6711–6721.

